

Multiscale Simulation of History Dependent Flow in Polymer Melt

Takahiro Murashima* and Takashi Taniguchi

*Department of Chemical Engineering, Kyoto University, Kyoto 615-8510, Japan and
CREST, JST, Kawaguchi, Saitama, 332-0012, Japan*

(Dated: November 24, 2018)

We have developed a new multiscale simulation technique to investigate history-dependent flow behavior of polymer melt, using a smoothed particle hydrodynamics simulation with microscopic simulators that account for the dynamics of entangled polymers acting on each fluid element. The multiscale simulation technique is applied to polymer melt flow passing a circular object in a two-dimensional periodic system. It is found that the strain-rate history-dependent stress of the polymer melt affects its flow behavior, and this stress memory causes nonlinear behavior even in the regions where $We \leq 1$.

PACS numbers: 83.10.Rs, 83.10.Mj, 83.60.Df, 83.80.Sg

Industrial products using polymeric materials have become increasingly integral to our lives. One of the important characteristics of thermo-plastic polymeric material is that it can be easily molded and processed by controlling its state from a solid to a melt, which is beneficial in a variety of practical applications. The melt state of polymeric material can exhibit a lot of characteristic phenomena, e.g., die-swell and rod-climbing[1], depending on the dynamic response of the polymer's microscopic internal states under an imposed strain or strain-rate.

Predicting the flow of polymeric fluid is difficult because the macroscopic flow behavior depends heavily on the dynamic behavior of the microscopic internal states, and the states of polymers with very high molecular weight are complex at the microscopic level. When a polymer melt consists of polymers with a molecular weight M higher than the entanglement molecular weight M_e , the polymer molecules are entangled with each other, and the relaxation time of the polymer conformation is long compared to that of dilute polymer solutions because of the entanglement. Therefore, it is difficult to predict the rheological behavior, even for a homogeneous bulk polymer melt, using molecular dynamics approaches without any coarse-graining procedures for the microscopic internal degrees of freedom. Reptation theory[2–4], in which a polymer chain is coarse-grained to a tube confined by the surrounding polymer chains, explains the complex behavior of polymer melt composed of monodisperse linear polymers. To apply the concept of a tube to a wider variety of polymers, the original reptation theory has been improved by introducing several important physical mechanisms[5–8]. Extended reptation theory based on the Fokker-Planck equation for tube segments succeeds in explaining many experimental results[5–8]. However, it is difficult to apply the theory to arbitrary polymer melts because it is too mathematically complex to incorporate the molecular pictures of polymers of arbitrary architectures into the Fokker-Planck equation. On the other hand, Langevin stochastic models based on reptation theory using the complex molecular configurations

have been developed and can reproduce the rheological properties of various polymeric materials with branches and/or molecular weight distributions[9–12]. These models use efficient numerical computation to predict the bulk rheology of polymer melts; however, they are not applicable to macroscopically inhomogeneous flows only by themselves. The macroscopic flow behavior of polymer melt is usually predicted using a fluid dynamics simulation with a constitutive equation that describes a nonlinear relationship between the stress and strain-rate fields to represent complex fluids without microscopic details. The Fokker-Planck equation of tube segments can also be regarded as a constitutive equation. No general constitutive equation that is applicable to arbitrary polymer melts exists because a general polymer melt has extremely complex molecular states, which make the stress response unpredictable even in simple flow patterns. As described above, each of the microscopic and macroscopic approaches has limited applications.

As an alternative to using a constitutive equation, we propose a new simulation technique that incorporates Langevin coarse-grained simulators[9–12] into a fluid dynamics simulation. This approach is a type of micro-macro simulations that were developed for polymer solutions in which the stress tensor of each fluid element is obtained from a microscopic simulation[13–15]. Our approach uses the Lagrangian fluid particle method[16] to solve the macroscopic fluid dynamics, and therefore the dependence of the stress on the history of the strain-rate is directly involved without a need for any special treatments to connect the Eulerian and Lagrangian schemes[13, 14]. When the polymer solution consists of long molecules without entanglement, the bulk behavior of the polymer solution can be treated as a single-body problem, while an entangled polymer melt is a full many-body problem. Therefore, a fully Eulerian technique such as the Brownian configuration field method[15] is difficult to apply to an entangled polymer melt system because it is difficult to describe the macroscopic advection of entangled polymers. In polymer melt flow, the advection of

microscopic internal states is essential to the description of the macroscopic flow behavior because the conformations of polymers at the microscopic level cause not only a linear response but also a nonlinear and/or retarded response, such as shear thinning and stress over-shoot. However, when considering a flow with symmetry, such as translational symmetry[17, 18], the fully Eulerian techniques can still be useful even for polymer melts.

To maintain the information pertaining to entanglement and deformation in polymers, we perform a Lagrangian fluid particle simulation in which each fluid particle has a microscopic level simulator that accounts for the internal states of the fluid particle[16]. Assuming that the polymer melt is an isothermal and incompressible fluid, the governing equations for the fluid particles that constitute the polymer melt are given by the following equations;

$$\rho_i \frac{d\mathbf{v}_i}{dt} = \nabla \cdot \boldsymbol{\sigma}_i - \nabla p_i + \mathbf{F}^b, \quad \frac{d\mathbf{r}_i}{dt} = \mathbf{v}_i, \quad (1)$$

$$\boldsymbol{\sigma}_i \equiv \boldsymbol{\sigma}_i(\boldsymbol{\kappa}_i), \quad (2)$$

and $p_i \equiv p_i(\{\rho_i\})$, where the velocity gradient tensor $\boldsymbol{\kappa}_i$ at the position of the i -th particle is defined as $\boldsymbol{\kappa}_i \equiv (\nabla \mathbf{v})_i^T$, and \mathbf{F}^b is a body force. These equations are solved using macroscopic variables, except for Eq. (2). The local stress tensor $\boldsymbol{\sigma}_i$ can be evaluated from microscopic variables that describe polymer dynamics under an instantaneous local strain-rate $\boldsymbol{\kappa}_i$.

The slip-link model[10, 11] is a simulation model that can accurately describe the dynamics of entangled polymers. The model is composed of confining tubes with some entanglement points, called slip-links, which confine a pair of polymers and represent effective constraints in virtual space. The average number of slip-links or entanglements on a polymer is represented as $Z \equiv M/M_e$. In the simulation, we trace the configurations of confining tubes constrained by the slip-links. The slip-links are relatively convected each other and the confining tubes are deformed according to the macroscopically obtained local velocity gradient tensor $\boldsymbol{\kappa}$. The reptations of polymers generate or eliminate slip-links. For given chain configurations, the stress tensor $\boldsymbol{\sigma}^p$ derived from deformations of entangled polymers is calculated from $\sigma_{\alpha\beta}^p = \sigma_e \sum_i \langle r_{i\alpha}^s r_{i\beta}^s / |\mathbf{r}_i^s| \rangle / a_s$ where a_s is the unit length of the slip-link model and $r_{i\alpha}^s$ is the α -component of the i -th tube segment vector connecting adjacent slip-links along a polymer. The unit of stress σ_e in the slip-link model relates to the plateau modulus G_N as follows: $\sigma_e = (15/4)G_N$ [11]. The slip-link model has two characteristic time-scales: the Rouse relaxation time τ_R and the longest relaxation time τ_d . The Rouse relaxation time τ_R and the longest relaxation time τ_d relate to Z as follows: $\tau_R = Z^2 t_e$ and $\tau_d \propto Z^{3.4} t_e$ [4, 11], where t_e is the time unit of the slip-link model. The contour length relaxation of a confining tube occurs on the time-scale of

τ_R , while the orientational relaxation occurs on the time-scale of τ_d . These two characteristic times appear in the stress relaxation.

Each polymer simulator describing a fluid particle computes the polymer configurations at each time step, and the recorded configurations are used as the initial conditions of the next time step. Typically, the macroscopic time unit t_{macro} and microscopic time unit t_{micro} have a large time-scale gap, and therefore the macroscopic time unit t_{macro} must be divided into $N t_{\text{micro}}$. Because the slip-link model used here is sufficiently coarse-grained and the time unit t_e can be the same as the time-scale of the macroscopic fluid t_{macro} , we employ $t_{\text{macro}} = t_{\text{micro}} \equiv t_e$.

Note that we set the local stress of the macroscopic fluid to $\boldsymbol{\sigma} = \boldsymbol{\sigma}^p + \boldsymbol{\sigma}^d$, where $\boldsymbol{\sigma}^d$ is an extra dissipative stress tensor. Because the slip-link model is a Langevin coarse-grained model based on reptation theory, microscopic dynamics smaller than a tube segment are treated as a random force exerted on a slip-link, and the contribution from the microscopic dynamics does not explicitly appear in the stress tensor of the slip-link model. We assume the dissipative stress $\boldsymbol{\sigma}^d$ to be the Newtonian viscosity $\eta_d \mathbf{D}$, where $\mathbf{D} \equiv \boldsymbol{\kappa} + \boldsymbol{\kappa}^T$ is a strain-rate tensor.

The main procedures of our simulation are summarized as follows: (1) Update $\{\mathbf{v}_i\}$, $\{\mathbf{r}_i\}$ at the macroscopic level. (2) Calculate $\{\rho_i\}$, $\{\boldsymbol{\kappa}_i\}$ at the macroscopic level. (3) Obtain $\{p_i\}$ from the density distribution $\{\rho_i\}$ at the macroscopic level. (4) Update the local slip-link model of the i -th fluid particle under the local strain-rate $\boldsymbol{\kappa}_i$ and then obtain $\boldsymbol{\sigma}_i$ from the resulting configuration of the slip-link model. This procedure is executed on each fluid element in turn. (5) Calculate $\{\nabla \cdot \boldsymbol{\sigma}_i\}$ and $\{\nabla p_i\}$ at the macroscopic level. (6) Return to (1).

We update $\{\mathbf{v}_i\}$, $\{\mathbf{r}_i\}$ by integrating Eq. (1). We calculate the density at the position of each particle in the new configuration using a method similar to the usual smoothed particle hydrodynamics technique[19]: $\rho_i = \sum_j m_j W(|\mathbf{r}_j - \mathbf{r}_i|, h)$, where m_i is the mass of the i -th particle and $W(|\mathbf{r}|, h)$ is a Gaussian-shaped function with cutoff length $2h$. The deviation of the local density from the initially constant density ρ_0 results in a local pressure force $-\nabla p$. To obtain the spatial derivative of the velocity field, stress field, and pressure field ($\nabla \mathbf{v}$, $\nabla \cdot \boldsymbol{\sigma}$, ∇p), we use a technique that was developed for modified smoothed particle hydrodynamics[20, 21].

To demonstrate the efficiency of the proposed multi-scale simulation, we consider a system in which the flow history can affect the flow behavior. One such system is a polymer melt that flows in the x -direction and passes an infinitely long cylinder oriented in the z -direction with a radius r_c . Because of the symmetry of the system, we can treat the system as two-dimensional, and the flow can be described as two-dimensional flow in the xy -plane. We assume a non-slip boundary condition for the velocity on the surface of the cylinder and periodic bound-

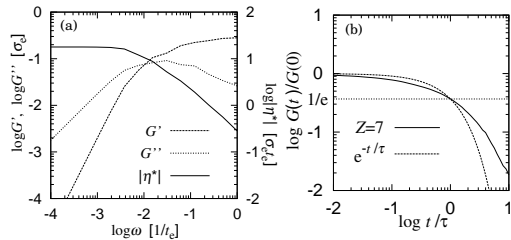


FIG. 1. (a) Rheological data and (b) relaxation modulus $G(t)$ obtained from the slip-link simulation with $Z = 7$ in the bulk. The storage modulus G' (broken line), the loss modulus G'' (dotted line), and the complex viscosity η^* (solid line) are plotted against the angular frequency ω in (a). The magnitude of the complex viscosity, $|\eta^*| = \sqrt{G'^2 + G''^2}/\omega$, is considered to be the shear viscosity η of the low shear-rate region (Cox-Mertz rule). The normalized relaxation modulus $G(t)/G(0)$ (solid line) and a single exponential curve with a relaxation time τ (broken line) are plotted against the normalized time t/τ in (b).

ary conditions at the boundaries of the system. The dimensionless parameters governing the problem are the Reynolds number $Re = \rho U r_c / \eta^0$, the Weissenberg number $We = \tau_d D_{xy}$, and the viscosity ratio η_d / η^0 , where U is the average flow velocity. The zero shear viscosity η^0 of the polymer melt is given by $\eta_p^0 + \eta_d$, where η_p^0 is the zero shear viscosity of a polymer melt described only by the slip-link model. From the rheological data shown in Fig. 1 (a), which were derived from the slip-link simulation with average $Z = 7$ entanglements in the bulk, we obtain the longest relaxation time $\tau_d \simeq 200t_e$ and the zero shear viscosity $\eta_p^0 \simeq 17.5\sigma_e t_e$. The cylinder radius r_c was set to $3a$, where a is the unit length in the fluid particle simulation, and we assign the unit mass m to all fluid particles. The wall of the cylinder consists of fixed fluid particles evenly spaced on the perimeter. Each fluid particle consists of 1000 polymers, enough to describe the bulk rheological properties of the polymer melt under an imposed shear and/or extensional deformation[16]. About 900 fluid particles with 1000 polymers each are evenly placed in the system; therefore, we need to simultaneously solve the dynamics of 900000 polymers. Because the diffusive motion of the center of mass of a single polymer is negligible compared to the translational motion of the center of mass of an ensemble of entangled polymers, we neglect any transportation of polymers between adjacent fluid particles. With this assumption, each slip-link simulation can be performed independently of the others, making parallel computing effective in this multiscale simulation.

Under the body force $\mathbf{F}^b / (\eta^0 / a t_e) = (5.0 \times 10^{-4}, 0)$, the flow becomes steady-state in about $1000t_e$. The average flow velocity in steady-state in this system is nearly equal to $(0.04, 0)a/t_e$ for a fully Newtonian flow $\eta^0 = \eta_d$ ($\sigma^p = 0$), and $(0.055, 0)a/t_e$ for a polymer melt flow with $Z = 7$ and $\eta_d / \eta^0 = 0.1$. In both cases, Re is less than 0.2,

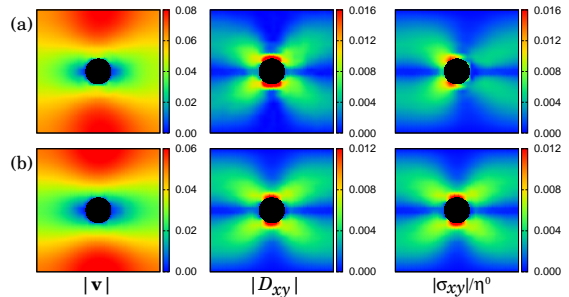


FIG. 2. Color contour maps of time-averaged magnitudes of the velocity field $|\mathbf{v}|[a/t_e]$, strain-rate $|D_{xy}|[1/t_e]$, and shear stress over the zero shear viscosity $|\sigma_{xy}|/\eta^0[1/t_e]$ for (a) the polymer melt with $Z = 7$ and $\eta_d/\eta^0 = 0.1$ and (b) the Newtonian fluid with $\eta^0 = \eta_d$ in steady-state.

and the flow is laminar. In the polymer melt flow case, the average flow velocity is higher than that of Newtonian flow, i.e., the flow exhibits shear thinning behavior. Because the strain-rate is larger than $1/\tau_d$ in the vicinity of the cylinder, We is larger than 1.

To investigate the velocity field \mathbf{v} , strain-rate D_{xy} , and shear stress σ_{xy} in steady-state, we employ a linear interpolation to transform the data at the particle positions into the values at regular lattice points and then time-average the data evaluated at the lattice points. To eliminate the noise of the data, the time-averaging was carried out from $1000t_e$ to $2000t_e$. Figure 2 shows the spatial distributions of $|\mathbf{v}|$, $|D_{xy}|$ and $|\sigma_{xy}|/\eta^0$ in steady-state for (a) the polymer melt with $Z = 7$ and $\eta_d/\eta^0 = 0.1$ and (b) the Newtonian fluid with $\eta^0 = \eta_d$.

Reflecting laminar behavior, the magnitudes of \mathbf{v} and D_{xy} in Fig. 2 appear to be nearly symmetric between the upstream and downstream regions unlike σ_{xy} . The shear stress σ_{xy} of the polymer melt exhibits an apparent asymmetry between the upstream and downstream regions. The nonlinear relationship between σ_{xy} and D_{xy} is observed near the cylinder where $We > 1$. If the asymmetry in the stress distribution is caused only by the nonlinear relationship, the stress distribution should be symmetric in the regions where $We \leq 1$. However, the asymmetry is also observed in the regions where $We \leq 1$.

It is assumed that the asymmetry in the stress distribution does not primarily originate from the nonlinear relationship between σ_{xy} and D_{xy} but rather due to the stress memory effect, because the stress on the polymer melt does not immediately vanish once the strain-rate is no longer applied. To clarify this hypothesis, we investigate the behavior of σ_{xy} and D_{xy} on two typical stream lines (A: solid line and B: broken line shown in Fig. 3 (a) in the region where $We \leq 1$, and then discuss the relationship between σ_{xy} and D_{xy} in these stream lines. Figure 3 (b) shows the σ_{xy} and D_{xy} distributions along these stream lines and plots them against the elapsed particle tracking time. The time origin $t = 0$ is set to t_{\min} ,

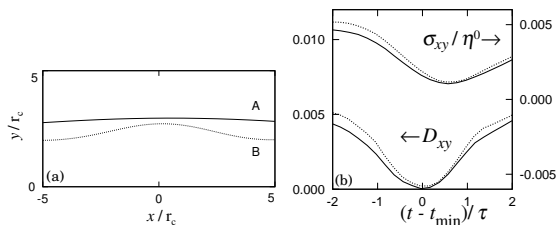


FIG. 3. Stream lines (solid line(A) and dotted line(B)) obtained from the time-averaged velocity field with particle tracking are plotted against position in (a). These stream lines are in the region where $We \leq 1$. The strain-rate D_{xy} and the shear stress σ_{xy} along the stream lines are plotted against the elapsed particle tracking time in (b). Each line type corresponds to each stream line.

when the strain-rate D_{xy} is at a minimum in each stream line. A nonlinear relationship between σ_{xy} and D_{xy} is not evident in either stream line because $We \leq 1$; however, the minimum of σ_{xy} appears to be shifted from that of D_{xy} by a time difference t_{Δ} . Applying a step shear strain $\gamma = 0.5$ to the slip-link model with $Z = 7$ in the bulk, we obtain the relaxation modulus $G(t) \equiv \sigma(t)/\gamma$ shown in Fig. 1 (b). The stress relaxation time τ is estimated to be $\tau \simeq 50t_e (\simeq \tau_R)$ when $G(t = \tau)/G(0) = 1/e$. The time difference t_{Δ} is found to be nearly equal to τ . In general, the viscoelastic stress relates to the shear-rate through the relaxation modulus according to the following equation: $\sigma(t) \propto \int_{-\infty}^t dt' G(t - t') \dot{\gamma}(t')$. If the stress does not depend on the flow history, the time difference t_{Δ} will be zero. However, the strain-rate D_{xy} and the shear stress σ_{xy} exhibit the apparent time difference t_{Δ} because of the stress memory with the relaxation time τ , not because of the nonlinear relationship between σ_{xy} and D_{xy} . Therefore, we conclude that the asymmetry in the stress distribution is caused by the history-dependent stress in the polymer melt. Using the Lagrangian particle method to trace and maintain the entire configurations of polymers, we have been able to describe the stress memory effect in the polymer melt flow.

We have developed a new multiscale simulation technique to investigate history-dependent flow behavior in polymer melt. This multiscale simulation consists of a modified smoothed particle hydrodynamics simulation and a slip-link model describing each fluid element. The multiscale simulation technique has been applied to polymer melt flow passing a circular object in a two-dimensional periodic system to demonstrate the effects of history-dependent stress. We have found that the strain-rate history-dependent stress in the polymer melt affects its flow behavior, and the stress field is retarded from the strain-rate field. Because the time difference t_{Δ} between the stress and strain-rate fields is nearly equal to the stress relaxation time τ , we conclude that the retardation of the stress field is due to the stress memory effect

in the polymer melt flow.

The presented multiscale simulation is applicable to various polymer melts, because the slip-link model or the alternative course-grained models[9, 12] can address a variety of polymer architectures, e.g., linear and/or branched polymers, polymer blends, and polydispersed polymers. The current multiscale simulation is advantageous because it employs a fully Lagrangian method at the macroscopic level, while conventional micro-macro techniques which have difficulties accounting for the macroscopic advection of microscopic internal states.

We thank Professor R. Yamamoto and Dr. S. Yasuda for their diligent discussions and helpful advice. We greatly appreciate Professor M. Doi and Professor J. Takimoto providing their source code of the slip-link model included in the *OCTA* system (<http://octa.jp/>).

* murasima@cheme.kyoto-u.ac.jp

- [1] D. V. Boger and K. Walters, *Rheological Phenomena in Focus*, Elsevier, (1993).
- [2] S. F. Edwards, *Proc. Phys. Soc.*, **92**, 9–16, (1967).
- [3] P.-G. de Gennes, *J. Chem. Phys.*, **55**, 572–579, (1971).
- [4] M. Doi and S. F. Edwards, *The theory of polymer dynamics.*, Oxford University Press, (1986).
- [5] D. W. Mead, R. G. Larson, and M. Doi, *Macromolecules*, **31**, 7895–7914, (1998).
- [6] G. Ianniruberto and G. Marrucci, *J. Rheol.*, **45**, 1305–1318, (2001).
- [7] G. Ianniruberto and G. Marrucci, *J. Non-Newtonian Fluid. Mech.*, **102**, 383–395, (2002).
- [8] A. E. Likhtman and R. S. Graham, *J. Non-Newtonian Fluid. Mech.*, **114**, 1–12, (2003).
- [9] Y. Masubuchi, J. Takimoto, K. Koyama, G. Ianniruberto, G. Marrucci and F. Greco, *J. Chem. Phys.*, **115**, 4387–4394, (2001).
- [10] S. Shanbhag, R. G. Larson, J. Takimoto and M. Doi, *Phys. Rev. Lett.*, **87**, 195502, (2001).
- [11] M. Doi and J. Takimoto, *Phil. Trans. R. Soc. Lond. A*, **361**, 641–652, (2003).
- [12] A. E. Likhtman, *Macromolecules*, **38**, 6128–6139, (2005).
- [13] M. Laso and H. Öttinger, *J. Non-Newtonian Fluid. Mech.*, **47**, 1–20, (1993).
- [14] P. Halin, G. Lielens, R. Keunings, and V. Legat, *J. Non-Newtonian Fluid. Mech.*, **79**, 387–403, (1998).
- [15] M. A. Hulsen, A. P. G. van Heel, B. H. A. A. van den Brule, *J. Non-Newtonian Fluid. Mech.*, **70**, 79–101, (1997).
- [16] T. Murashima and T. Taniguchi, *J. Polym. Sci. B*, **48**, 886–893, (2010).
- [17] S. Yasuda and R. Yamamoto, *Euro. Phys. Lett.*, **86**, 18002, (2009).
- [18] S. Yasuda and R. Yamamoto, *Phys. Rev. E*, **81**, 036308, (2010).
- [19] J. Monaghan, *Rep. Prog. Phys.*, **68**, 1703–1759, (2005).
- [20] G. Zhang and R. Batra, *Comput. Mech.*, **34**, 137–146, (2004).
- [21] M.B. Liu, W.P. Xie, and G.R. Liu, *Appl. Math. Model.*, **29**, 1252–1270, (2005).